AIAA JOURNAL
Vol. 33, No. 12, December 1995

Shape Optimization with *p* Adaptivity

Raviprakash R. Salagame* and Ashok D. Belegundu†
Pennsylvania State University, University Park, Pennsylvania 16802

The *p* method of analysis, when used with shape optimization, has certain advantages over the *h* method. The method of *h* adaptivity results in fine meshes with small elements in areas of stress concentration. The presence of these small elements prevents the shape from changing significantly during optimization due to mesh distortion. The *p*-adaptive method uses relatively large sized elements, and adaptivity is achieved by increasing the polynomial order of the shape functions rather than by introducing small elements as in the *h* method. Thus, the *p*-adaptive method allows for greater shape changes without sacrificing the accuracy of the analysis. A methodology is developed in this paper to integrate *p*-adaptive analysis with shape optimization for general velocity fields. The key contributions lie in an easily implementable shape update strategy and an adaptive scheme to locally increase the polynomial order based on error indicators. Numerical results show that significant shape change is achievable prior to serious mesh distortion. In addition, need for an *h–p* adaptive strategy rather than a pure *p*-adaptive strategy is also highlighted.

Introduction

STRUCTURAL shape optimization has been an active area of research for the last two decades. Most of the earlier work in this field focused on developing velocity fields, shape sensitivity analysis, and numerous practical applications in automotive and aerospace industry (Refs. 1–4, to name a few). With the parallel development of adaptive methods for finite element analysis, the focus shifted to using adaptive analysis for shape optimization. Most of the research so far in this direction has been on using the *h* method. In this method, the degree of the shape functions is fixed, usually linear or quadratic. Adaptivity is implemented by introducing additional small sized elements in regions of high-stress gradients, with the use of a mesh generation program.

The use of *p* elements for shape optimization is motivated by the following benefits that these elements offer.

1) The *p* elements are large in size. This implies that large shape changes can take place during optimization before element distortion and degeneracy become critical. Moreover, *p* elements are known to tolerate large aspect ratio and skew angles.

2) The mesh topology remains the same during the adaptivity process (only *p* is changed).

3) When *p* is increased, the entire stiffness matrix need not be recomputed, due to the hierarchic nature of shape functions. This leads to more efficient computation procedures.

The presented approach is based on the natural method. The shape is described by a collection of basis shapes, the linear combination of which constructs the optimum shape. Our design variables are the coefficients of the basis shapes in this linear combination. Basis shapes can be generated by specifying boundary displacements or by perturbing the geometric model. A general approach for shape update and for generating velocity fields has been developed in the present method. The idea is to generate velocity fields in parametric form that get directly added to the parametric equations describing the geometry of the element sides. This results in a continuous shape update procedure, which can be quickly implemented into computer codes.

The *p* method implemented with the adaptive scheme is based on the work of Szabo and Babuska.[5] However, an algorithm to locally increase the polynomial order has been developed as a part of the analysis module. This polynomial upgrade is based on error indicators, and the convergence check is based on global strain energy. The details of the *p*-adaptive analysis are summarized in a later section.

Several numerical problems are solved to illustrate the methodology. Although the focus in this paper is restricted to two-dimensional problems, the method is extendable to three-dimensional problems.

Earlier Work on *p*-Adaptive Techniques in Shape Optimization

The use of *p* elements in shape optimization is a relatively new area of research. Basic ideas in this direction were first proposed by Schiermeier and Szabo.[6] This work is more of a case study than a systematic optimization. The focus is on the assurance of reliability and accuracy of computed data. The shape optimal design procedure is interactive in the sense that the designer chooses the design parameters based on the information generated in the analysis cycle. This paper was followed by the work of Shyy et al.,[7] who formulated a shape optimal design problem rigorously using *p* elements. In their work, design elements are used. Design and analysis models are very closely related since large elements are used. The analysis is done at a specified value of *p*, which is usually the highest implemented value. Recently, King and Thanedar[8] developed a shape optimization methodology with *p* elements, which has been implemented into a commercial software program. This work is based on the geometric method of shape parametrization and uses adaptivity to increase the element order. The user parametrizes the mesh by associating the design variables to parametric curves. A comparison of the *p*-element-based shape optimization with the CSG approach and the reduced basis approach has been recently published by Kodiyalam and Thanedar.[9] The methodology developed in this paper is different from the cited approaches in the sense that it is based on the basis vector approach and, hence, allows more general shape variations.

p-Adaptive Analysis

The adaptive method developed here works as follows. The structure is analyzed at an initial value of *p*, say, $p = 2$. An error indicator is used to identify the element sides for which *p* is increased maintaining compatibility across elements. The structure is reanalyzed, and the error in strain energy is estimated. The iteration is stopped when the difference in normalized strain energy between successive iteration is small. A convergence to within 2–5% in the normalized strain energy is found to give acceptable results.

The error indicator is based on two considerations: the residual inside the element domain (called *r* indicator) and the traction jump across interelement boundaries (called *t* indicator). Error indicators of this type have been widely used in the literature.[10,11] The error indicators implemented here were proposed by Szabo.[12] However, the refinement algorithm based on the error indicators is a part of the current work.

Received July 20, 1994; revision received Feb. 24, 1995; accepted for publication Feb. 28, 1995.

*Graduate Student, Department of Mechanical Engineering; currently at IBM Almaden Research Center, San Jose, CA 95120.

†Associate Professor, Department of Mechanical Engineering.

Error Indicators

The r indicator is evaluated by integrating the residual over the element domain. The residual is the error obtained by inserting the finite element response into the governing differential equation, generally written as

$$r = Lu_{\text{FE}} - f$$

where L is the differential operator, u_{FE} the finite element displacement solution, and f the load vector. For solid mechanics problems in two or three dimensions, the governing differential equation is the equilibrium equation. The r indicator is defined as

$$e_r = \frac{A_e}{p^\alpha E} \int_{A_e} \left(r_1^2 + r_2^2\right) t \, dA \tag{1}$$

where r_1 and r_2 are the residuals along the x and the y directions, A_e is the area of the element, t is the element thickness, E is Young's modulus, p is the polynomial order and α a constant found from numerical experiments.

The t indicator is evaluated by integrating the traction jump across interelement boundaries. Specifically, it is defined as

$$e_t = \frac{\sqrt{A_e}}{p^\beta E} \int_{\Gamma_k} \left(t_1^2 + t_2^2\right) t \, dS \tag{2}$$

where t_1 and t_2 are the traction jumps across an interelement boundary Γ_k along the x and y axes and β is a constant found from numerical experiments. In the present work, we have used $\alpha = 3$, $\beta = 2$ (Ref. 12).

***p*-Refinement Strategy**

First, the error indicators are normalized with respect to the maximum value in the entire domain. Two options are provided: 1) use of t indicator alone and 2) use of t indicator in conjunction with r indicator. In case of option 1, the value of p is incremented by 1 on those sides for which

$$\text{tol1} < (e_t)_{\text{normalized}} < \text{tol2} \tag{3}$$

and it is incremented by 2 if the indicator is more than tol2. If the error indicator is less than tol1, then p is unchanged. The values of tol1 and tol2 are set to 0.3 and 0.7 in the present work. These limits represent a midrange in which most of the error indicators are likely to lie. Hence, p is incremented by 2 for the side with the highest numerical value of the error indicator.

In the case of option 2, the preceding rule is used to identify the elements which have to be refined, but the tolerances, tol1 and tol2 are made tighter. For example, if e_r lies between tol1 and tol2, then the corresponding element is selected for refinement and the rule is used again for the sides of that element to increment p.

For most problems, the t indicator gives a good idea of regions for refinement. When large elements are used in regions where the stresses vary sharply, however, it is necessary to look at the residual errors as well.

Analysis at a *p* Distribution

The analysis at a p distribution determined during the adaptive process is based on the work of Szabo and Babuska.[5] A summary of the approach, especially the geometric mapping technique, is given here.

The geometric and the displacement functions are independently mapped in the p method. The displacement components are given by

$$u(\xi, \eta) = \sum_{j=1}^{\text{num}} N_j a_j$$

$$v(\xi, \eta) = \sum_{j=1}^{\text{num}} N_j a_{j+\text{num}} \tag{4}$$

where N_j are the shape functions, a_j the shape function amplitudes, and num are the number of shape functions. The shape function amplitudes generally do not represent physical displacements. The

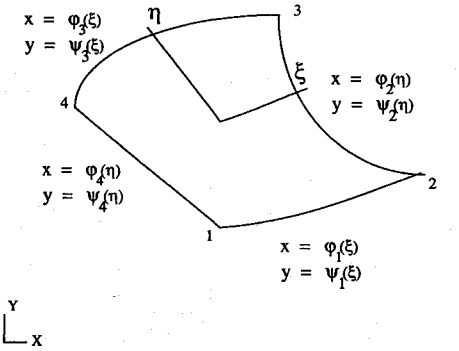

Fig. 1 Four-noded quadrilateral *p* element.

shape functions are proportional to the integrals of the Legendre polynomials. They are hierarchic in nature and yield solutions which monotonically converge in the energy norm as p is increased. The hierarchic property means that the solution obtained at p is imbedded in the solution obtained at $p + 1$. In other words, the stiffness matrix for p is contained in the stiffness matrix for $p + 1$. If the degrees of freedom are properly arranged, the stiffness matrix at $p + 1$ appears as

$$\begin{bmatrix} K_{(n\times n)} & K_{(n\times nd)} \\ K_{(nd\times n)} & K_{(nd\times nd)} \end{bmatrix}_{[(n+nd)\times(n+nd)]}$$

where $K_{(n\times n)}$ is the stiffness matrix for the order p and nd degrees of freedom are added when p is increased to $p + 1$. This implies that $K_{(n\times n)}$ need not be recalculated during adaptivity.

The geometric mapping is based on the use of blending functions. To understand this, consider a two-dimensional 4-noded quadrilateral element as shown in Fig. 1. The element sides are described by parametric functions as shown in the figure. The coordinates of any point inside the element is described by a mapping function in which (x_k, y_k) are the coordinates of the kth node of the element,

$$x(\xi, \eta) = \frac{(1-\eta)}{2}\varphi_1(\xi) + \frac{(1+\eta)}{2}\varphi_3(\xi) + \frac{(1-\xi)}{2}\varphi_4(\eta) + \frac{(1+\xi)}{2}\varphi_2(\eta) - \sum_{i=1}^{4} \frac{1}{4}(1+\xi_i\xi)(1+\eta_i\eta)x_i$$

$$y(\xi, \eta) = \frac{(1-\eta)}{2}\psi_1(\xi) + \frac{(1+\eta)}{2}\psi_3(\xi) + \frac{(1-\xi)}{2}\psi_4(\eta) + \frac{(1+\xi)}{2}\psi_2(\eta) - \sum_{i=4}^{4} \frac{1}{4}(1+\xi_i\xi)(1+\eta_i\eta)y_i \tag{5}$$

The mapping given by Eq. (5) is simple coons' patch defined with four boundary curves.

The finite element analysis equations are formulated using the principle of virtual work. The equations are solved for the amplitudes a_j. Displacement at any point are then calculated from Eq. (4). Stresses, strains, and strain energy are computed in the same way as in the h method. Handling boundary conditions and traction loads using p elements requires certain special considerations which will not be outlined here.

Shape Update and Velocity Fields

At the end of each optimization iteration, the shape is updated by modifying the finite element model using velocity fields. Since the finite element model in the p method involves geometric description of the sides, a nodal coordinate update alone is insufficient, as used in the past. A general approach for shape update and for generating velocity fields has been developed here for p elements. The method involves generation of continuous velocity fields in parametric form, which get directly added to the parametric equations describing the geometry of the element sides. The velocity fields in the present work are generated by the displacement approach. However, computer aided design (CAD) based approach can also be used within the framework of this update procedure.

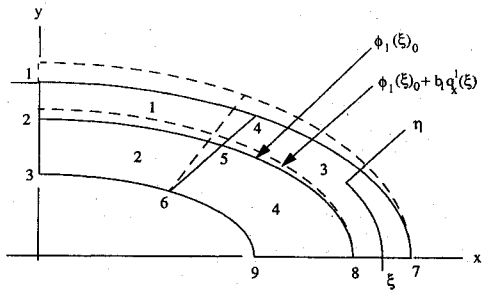

Fig. 2 Update of element sides in parametric form.

In the h method, the nodal coordinates can be updated using the equation[4]

$$G_n = G_{n-1} + \sum_{i=1}^{ndv} b_i q^i \tag{6}$$

where G_n is the vector of nodal coordinates at the end of the nth iteration, G_{n-1} is the vector of nodal coordinates at the end of the $(n-1)$th iteration, b_i are the ndv design variables, and the vectors q^i are the corresponding velocity fields ($3nn \times 1$). The vectors G are of dimensions ($3nn \times 1$) where nn are the number of nodes.

Conceptually, the form of the update equation for p elements is identical to that given by Eq. (6). But the vector G is replaced by the parametric equation of the element side. Thus, the corresponding velocity field q is also a continuous function rather than a vector. This equation is applied to all of the element sides to update its representation. The nodal coordinate update in Eq. (6) is just a special case of this general form. The updated sides are then used in the mapping by the blending function method to represent the new shape. For example, side 1 of the element (see Fig. 1) at the end of nth iteration is updated by

$$\begin{aligned} \varphi_1(\xi)_n &= \varphi_1(\xi)_{n-1} + \sum_{i=1}^{ndv} b_i q_x^i(\xi, -1) \\ \psi_1(\xi)_n &= \psi_1(\xi)_{n-1} + \sum_{i=1}^{ndv} b_i q_y^i(\xi, -1) \end{aligned} \tag{7}$$

where the indices x and y on q represent the coordinate axes. The update is illustrated graphically in Fig. 2.

Equation (7) can be expressed in terms of the initial shape for which the parametric form is known beforehand. The resulting equation is

$$\begin{aligned} \varphi_1(\xi)_n &= \varphi_1(\xi)_0 + \sum_{k=1}^{n} \left\{ \sum_{i=1}^{ndv} b_i q_x^i(\xi, -1) \right\}_k \\ \psi_1(\xi)_n &= \psi_1(\xi)_0 + \sum_{k=1}^{n} \left\{ \sum_{i=1}^{ndv} b_i q_y^i(\xi, -1) \right\}_k \end{aligned} \tag{8}$$

Similar equations can be written for the other three sides as well as the nodal coordinates. Let

$$\begin{aligned} \varphi 1(\xi)_n &\equiv \varphi 1(\xi)_0 + U_1(\xi) \\ \psi 1(\xi)_n &\equiv \psi 1(\xi)_0 + V_1(\xi) \end{aligned} \tag{9}$$

where U and V represents the continuous motion of the side, which can be obtained by comparing Eqs. (8) and (9). In the preceding equations, $\varphi_1(\xi)_0$ and $\psi_1(\xi)_0$ are the parametric equations of the element sides of the initial design, which is described by the user. As the shape changes, the additional terms are computed using the velocity fields and the design variables as described by Eqs. (8) and (9). The geometric mapping for the shape at the end of nth iteration is now expressed using the blending function method as discussed earlier. The mapping function for the x coordinate is given by

$$\begin{aligned} x(\xi, \eta)_n &= x(\xi, \eta)_0 + \frac{(1-\eta)}{2} U_1(\xi) + \frac{(1+\eta)}{2} U_3(\xi) + \frac{(1-\xi)}{2} \\ &\times U_4(\eta) + \frac{(1+\xi)}{2} U_4(\eta) - \sum_{i=1}^{4} \frac{1}{4}(1+\xi_i\xi)(1+\eta_i\eta)u_i \end{aligned} \tag{10}$$

where u_i is the motion of the ith node in the x direction from its initial position. Similar equations follow for $y(\xi, \eta)$.

The shape update procedure described by Eqs. (9) and (10) is very attractive from the implementation point of view. The parametric equations of the side at any intermediate stage of the optimization are expressed as initial shape plus some cumulative displacement. This means that if the intermediate values of the design variables and the velocity fields are stored, any intermediate shape can be instantly generated. It is not necessary to physically update the shape at the end of every iteration except for visualization. This process becomes even more simple if the velocity fields are generated offline. In many problems, however, the geometric constraints imposed on the shape of the structure require that the velocity fields be generated online or at the end of every iteration.

Another feature of the update equation is that the velocity field is also a parametric function of the natural coordinates. This implies that the velocity fields generated by geometric methods can also be easily incorporated into the equation. The CAD modelers usually represent surfaces using parametric surface patches. These surface patches are in turn constructed by the curves represented in parametric form. Once the geometry is parametrically described, the given form of shape update is applicable.

To perform finite element analysis at intermediate shapes, we need to evaluate the derivatives of the geometric mapping functions. These derivatives are also obtained by directly differentiating Eq. (10). This computation requires differentiating the velocity fields with respect to the parametric variables.

Velocity Fields

The velocity fields are generated using the natural method. The auxiliary model consists of the same finite element mesh as the primary model but has different boundary conditions and loads. The boundary displacements are generated by specified displacement functions wherever necessary. The auxiliary analysis is usually done at a low value of p, such as $p = 2$, and without adaptivity. Thus, in our examples, the functions q_x and q_y [see Eq. (8)], are polynomials of degree p. Two kinds of specified displacements are allowed in the model as explained next.

Specified Polynomial Displacement

Here, a polynomial function is specified on a side so that it satisfies certain form preserving constraints. As an example, consider the bracket shown in Fig. 3 (Ref. 3).

In this problem, the outer boundary is allowed to change, keeping the radius of the three corner arcs the same. The shape of the slot is also changed retaining the symmetry about the central vertical

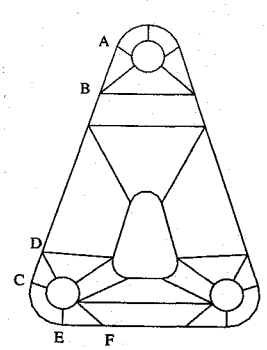

Fig. 3 Bracket subjected to a load.

axis. For the initial design shown in the figure, straight sides such as AB, CD, and EF are tangential to the circular arcs which they join. It is intended that as the shape changes, this tangency be maintained. This condition is achieved by specifying a cubic polynomial displacement function of the type

$$u_n(s) = b_0 + b_1 s + b_2 s^2 + b_3 s^3 \qquad s = [\xi, \eta]$$

where u_n is the displacement normal to the side AB. The unknowns in the preceding equation can be computed from the specified end conditions: two displacements and two slopes. Specified displacement functions of the form described have been implemented with the analysis module to broaden the possibility of generating complex velocity fields.

Boundary Displacement by Using Geometric Representation

The boundary displacements can also be generated by moving the control points of the curves which are parametrically described by Bezier curves or B splines. The control points can be moved in a specified way that preserves the geometric constraints. Since velocity fields are described using parametric equations, this method of generating velocity fields is very attractive for integrating shape optimization with CAD geometry.

The shape update and velocity field generation have been integrated with an optimizer that is based on the feasible direction method. Attention is given to handling distortion of the elements using the method presented by Zhang and Belegundu.[13] Sensitivity analysis is done by the method of finite difference. We discuss several examples in the next section.

Numerical Examples

The examples presented here involves a large change in shape, a change that could quickly distort an h-element mesh. The adaptivity is done with an initial uniform p distribution of $p = 2$. The distortion is controlled during line search using a distortion parameter (DP) (Ref. 13). The need for using adaptive p method is also illustrated.

Example 1: Connecting Rod

This example has been used by Bugeda and Oliver[14] to verify their optimization strategy. The authors have solved the problem with the h-adaptive mesh refinement strategy using a few key nodal coordinates as design variables. The problem is solved here with two design variables.

The objective is to minimize the volume of the connecting rod subject to a maximum allowable von Mises stress of 200 MPa. The component is shown in Fig. 5 basis shape 1 along with the p-element mesh. Because of the symmetry, only a quarter of the model is used in the problem. A parabolic normal load is assumed at the pin end with a total value of the load equal to 4 kN. The material properties are Young's modulus = 200 GPa and Poisson's ratio = 0.3. Stress constraints are imposed at the 16 Gauss points (4×4) of each element totaling 144 stress constraints. Two design variables are used in the problem to describe shape variations. One of the design variables represents a change in the height (initial value = 37.5 mm) and the other a change in the outer radius of the end (initial value = 30 mm). The basis shapes are shown in Fig. 3. The first basis shape is generated by specifying a displacement normal to the outer boundary, which is not constrained in the primary model. The second basis shape is generated by applying traction load to horizontal part of the outer boundary. These two basis shapes address all of the design requirements specified in the reference.

During most of the optimization iterations, the adaptive process converged in about 2–3 iterations. The optimum shape shown in Fig. 6 is obtained after 12 iterations. The weight reduction is about 71% from the initial weight with one active stress constraint near the top of the hole.

To verify the optimum shape, it is remeshed and the optimization performed again. As a result of the new mesh, the maximum stress, which is active at the end of 12th iteration, was higher by about 10%. This difference is attributed to two reasons: 1) the change in mesh topology, resulting from the different location of the Gauss points at which the stress constraints are evaluated and 2) the distorted

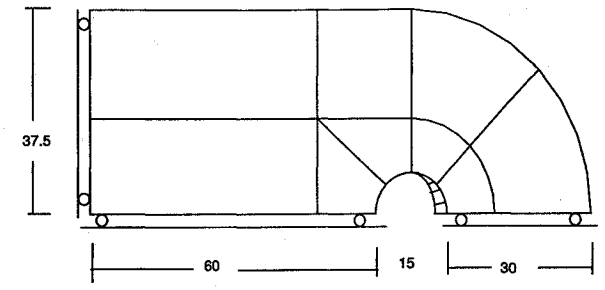

Fig. 4 Connecting rod, 9 element mesh: all dimensions in mm; t = 5 mm.

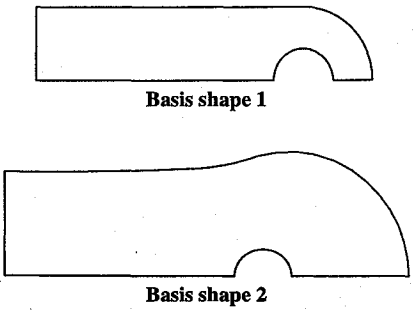

Fig. 5 Design variables for connecting rod.

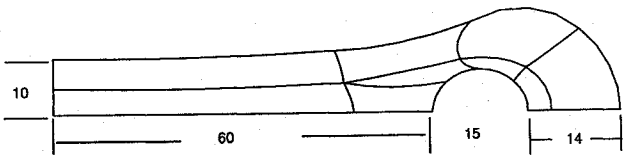

Fig. 6 Optimum shape after 12 iterations.

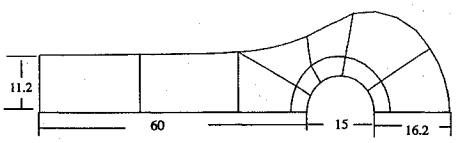

Fig. 7 Optimum shape after remesh-optimization, 6 iterations.

element in the region of high stresses. The first reason is typical of h refinement and this behavior is further elaborated on here.

When an h-adaptive scheme is used, the adaptivity alters the topology of the mesh, because the locations of the Gauss points at which the stress constraints are evaluated is different. In the absence of any extrapolation techniques or special methods of stress constraint formulations, i.e., if we simply enforce stresses at Gauss points as is usually done, we observe this jump in stress constraints. In contrast, in p adaptivity, the Gauss point locations do not change as a result of refinement (increase in polynomial order). Consequently, stress constraints enforced at Gauss points will have smoother convergence due to adaptivity. In defense of the h method, however, it can be stated that this smooth convergence probably might be achievable if the stress constraint locations are kept track of as the mesh topology changes. Thus, stress constraints should be enforced at some fixed locations instead of at Gauss points. Practically doing this is very difficult and requires special formulations. In this respect, p adaptivity surpasses h adaptivity for shape optimization problems.

The violation of the stress constraint in this problem is corrected by further shape modification through optimization using similar basis shapes. The resulting final optimum shape is shown in Fig. 7. The weight increase for the stress correction is about 12% of the first optimum design. Hence, the overall total weight reduction from the initial design is about 66%.

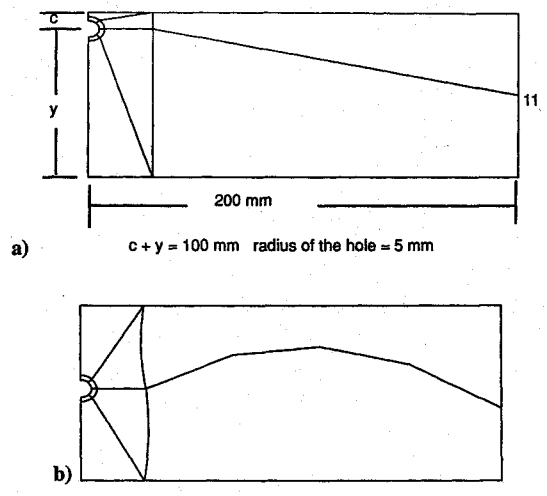

Fig. 8 Half-symmetry model: a) initial location, with p elements, and b) optimum location after 15 iterations.

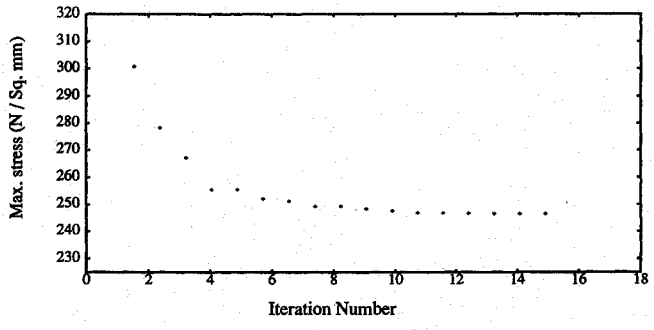

Fig. 9 Objective function history for example 2.

Example 2: Location of a Circular Hole in a Rectangular Plate

The objective here is to minimize the maximum stress around the hole. The design variable is the location of the hole along the y direction. The p-element mesh on a half-symmetry model is shown in Fig. 8. Small elements are used around the hole since stress variations are steep in that region. The single basis shape is obtained using a specified displacement on the edges of the elements around the hole along the y direction. To restrain rigid body modes, node 11 is fixed in the y direction. This point was chosen since the y displacement of node 11 becomes smaller and smaller as the hole is moved toward the center. Hence, the stress results around the hole are not seriously affected. A normal pressure load of 100 MPa is applied along the horizontal direction. The material properties are Young's modulus = 200 GPa, Poisson's ratio = 0.3, and allowable stress = 800 N/mm^2. The optimum location is also shown in Fig. 7 The ratio c/y for the initial and the optimum shapes are 0.11 and 1.05, respectively. The theoretical solution would be $c/y = 1.0$.

The objective function history (Fig. 9) shows that the optimum is quickly reached, but the tail end is longer due to a tighter tolerance of the optimizer. The optimum shape for this problem was also remeshed and analyzed. The maximum stress for the new mesh is very close to that for the optimum shape highlighting the accuracy of the analysis. Figure 9 also illustrates that the maximum stress varies smoothly with the change in design variable. The use of the h method for this problem would require intermediate remeshing. Such remeshing could disturb the maximum stress values and the convergence of the optimizer.

Example 3: Bracket

This problem was originally solved by Bennett and Botkin[3] using h adaptivity. The objective is to minimize the volume of the bracket keeping the maximum von Mises stress below a specified value. This problem poses considerable challenges when using the h method because of mesh distortion. The initial shape is shown in Fig. 10 along with the p-element mesh.

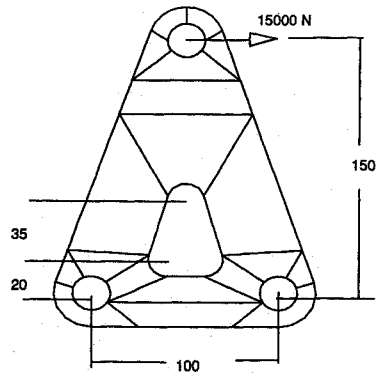

Fig. 10 Initial shape of the bracket, with the p-element mesh: all dimensions in mm; all hole radii are 10 mm.

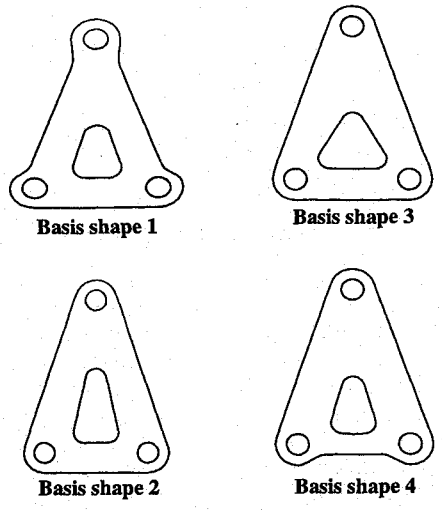

Fig. 11 Four basis shapes for the bracket problem.

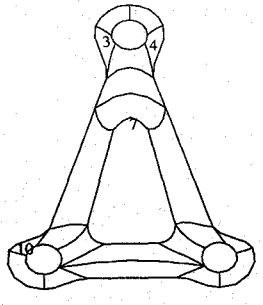

Fig. 12 Optimum shape of the bracket, 11 iterations.

The design constraints require that the symmetry be maintained and the size of the circular holes be constant. Accordingly, four basis are generated as shown in Fig. 11. As discussed in the preceding section on velocity fields, the corners are kept smooth by specifying a cubic variation of the boundary such that the slopes are continuous.

The bracket is loaded along the horizontal direction at the center of the top hole while it is held at the center of the two bottom holes. The material properties are same as that for the preceding example.

The constraints are imposed on the von Mises stress at 4×4 Gauss points of all of the elements except those touching the top hole.

The adaptive analysis is done starting from a uniform p distribution of $p = 2$ for all of the sides. A strain energy convergence of 5% is used. The first optimization run terminated with one active stress constraint with the shape shown in Fig. 12. The weight reduced by about 42%.

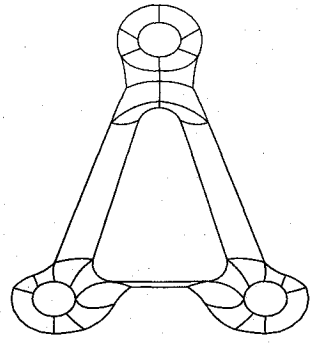

Fig. 13 Optimized shape after stage 2.

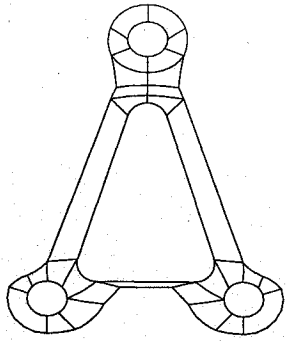

Fig. 14 Optimum shape after stage 3.

Effect of Mesh Distortion and Remeshing

Since some of the elements in the optimum shape have large distortions (for example, elements numbered 3, 4, and 10, Fig. 12), the domain is remeshed manually. The p-adaptive analysis with the new mesh shows that the maximum stress constraint, which is active at the last iteration, is now inactive, but two other constraints are violated by about 8%. This variation indicates that there is a significant jump in stresses as a result of remeshing (h refinement) and this behavior has already been discussed in the connecting rod example. The fact that the stress jump here is significant demonstrates that even with the p method, distortion effects are unavoidable when large shape changes are involved. The amount of shape change before distortion occurs, however, is greater than that which is attainable by the h method. Thus, we can conclude that a robust shape optimization approach should incorporate an h–p adaptive strategy than a pure p-adaptive strategy.

The optimization is continued with the new mesh. This second-stage optimization converged in 14 iterations. The optimum shape is shown in Fig. 13. At the end of this optimization, none of the stress constraints are found to be active, although one of the constraints is very close to the constraint band. The distortion constraint is active, however, which restricted further progress of optimization. The distortion is caused by the thinning of the element at the bottom of the bracket as shown in the figure.

The domain is now rezoned manually by moving some of the nodes so that the shapes of the distorted elements are corrected. The optimization is continued again for the third time (stage 3) without the design variable which moved the horizontal boundary upward. After manual rezoning, the analysis shows a constraint violation by 5%. This is again a combined effect of distortion and modified mesh. Stage 3 optimization converged in 18 iterations to the final optimum shape shown in Fig. 14. For this stage, three stress constraints are active, but there distortion limit is inactive.

The objective function history (change in volume) is shown in Fig. 15. The total reduction in weight is about 54.0%, which compares with the results from Ref. 14 (57%). The total reduction is achieved with two mesh refinements, however, which illustrates the fact that larger shape change is possible with the p method before mesh distortion affects the accuracy of analysis results.

Need for Adaptivity

In all of the examples described so far, the analysis is done using adaptively obtained p distribution. The need for adaptivity has been

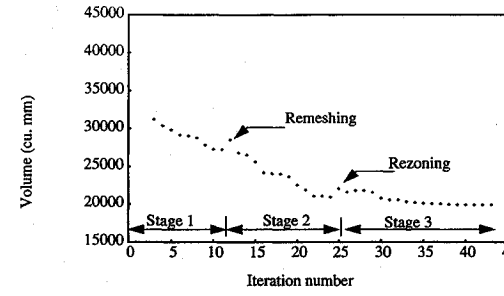

Fig. 15 Objective function history for the bracket problem.

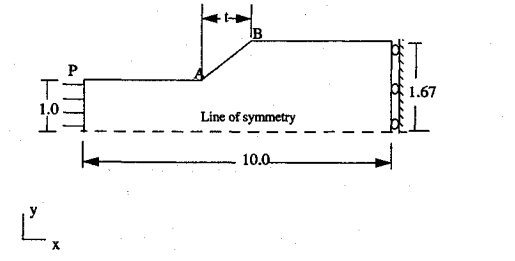

Fig. 16 Tension strip with a fillet; all dimensions in inches.

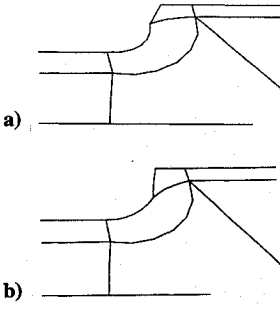

Fig. 17 Effect of adaptivity on shape: a) optimum shape without adaptivity and b) optimum shape with adaptivity.

implicitly assumed, however, because of the size of the elements. In this section, the effect of analysis at a fixed lower value of p on the optimum designs is studied. If the fixed value is high enough, the stress constraints are computed fairly accurately and the optimum shape is not likely to be affected, but the computational cost will be very high.

The problem is to design a fillet for minimizing the maximum stress.[15] The objective here is to find the shape of the curve AB (Fig. 16) for a fixed transition length t so that the maximum stress on the boundary AB is minimized.

The transition length t is set to 0.5 in. The fillet is divided into two regions. The region 1–3, which belongs to element E3 is modeled as a quadratic Bezier curve with control points 1, 2, and 3. The remaining part of the curve, 3–4, which belongs to element E5 is a straight line.

Three design variables are defined for this problem, the x and y coordinates of the control point 3 and the x coordinate of the control point 2. The analysis is done at a fixed value of p equal to 2 for all of the sides. All of the other parameters remain the same. The optimum shapes with and without adaptivity are shown in Fig. 17. The difference in the two shapes is obvious from the figure. In the case of optimization without adaptive analysis, the stress constraints are not computed very accurately. Thus, adaptive analysis plays an important role in this problem.

The other examples discussed in this section are also solved without adaptivity. In the case of example 2, the optimum hole location with and without adaptivity is found to be nearly the same. When adaptivity is not used for the analysis, however, the maximum stress at the initial and the optimum designs is overestimated by 20%. For the bracket problem (example 3), the optimum shape is not affected significantly due to analysis at a fixed p (equal to 2 for all of the sides). This behavior is most likely due to the fact that the initial mesh is not very coarse.

Conclusions

A methodology to perform shape optimization using p-adaptive finite elements has been developed in this paper. The primary contribution to shape optimization literature is the development of a shape update scheme using displacement-based velocity fields and basis vector approach. This update procedure uses an initial parametric representation and adds shape modifications which are functions of the velocity fields. It is shown that the use of p elements for shape optimization allows specification of more general and complex velocity fields. It is also shown that the use of p elements allows greater shape change before distortion effects become critical.

As a part of the integrated shape optimization scheme, a reliable p-adaptive analysis procedure has been developed. The concept of local error indicators has been borrowed from the literature, and a refinement scheme has been developed.

The numerical examples support the claim that the p-adaptive method can accommodate larger shape changes before mesh distortion becomes critical. The problem of distortion, however, is not entirely avoided. Hence, remeshing and/or rezoning is still needed, although at a much later stage and less frequently than with the h-adaptive shape optimization. This fact suggests an adaptive h–p scheme. In such a method, the mesh would be modified intermittently to capture the variation of shape, and the analysis would be done using p adaptivity with coarse elements.

References

[1]Zienkiewicz, O. C., and Campbell, J. S., "Shape Optimization and Sequential Linear Programming," *Optimum Structural Design*, edited by R. H. Gallagher and O. C. Zienkiewicz, Wiley, New York, 1973, pp. 109–126.

[2]Imam, M. H., "Three-dimensional Shape Optimization," *International Journal for Numerical Methods in Engineering*, Vol. 18, 1982, pp. 661–673.

[3]Bennett, J. A., and Botkin, M. E., "Structural Shape Optimization with Geometric Description and Adaptive Mesh Refinement," *AIAA Journal*, Vol. 23, No. 3, 1985, pp. 458–464.

[4]Belegundu, A. D., and Rajan, S. D., "A Shape Optimization Approach Based on Natural Design Variables and Shape Functions," *Computer Methods in Applied Mechanics and Engineering*, Vol. 66, 1988, pp. 87–106.

[5]Szabo, B. A., and Babuska, I., *Finite Element Analysis*, Wiley, New York, 1991.

[6]Schiermeier, J. E., and Szabo, B. A., "Interactive Design Based on the p-Version of the Finite Element Method," *Finite Elements in Analysis and Design*, Vol. 3, 1987, pp. 93–107.

[7]Shyy, Y. K., Fleury, C., and Izadpanah, K., "Shape Optimal Design Using Higher Order Elements," *Computer Methods in Applied Mechanics and Engineering*, Vol. 71, 1988, pp. 99–116.

[8]King, R. P., and Thanedar, P., "Shape Optimization Using Adaptive Higher Order Finite Elements," *Proceedings of the AIAA/ASME/ASCE/AHS/ASC 33rd Structural Dynamics and Materials Conference*, AIAA, Washington, DC, Vol. 5, 1992, pp. 2700–2707.

[9]Kodiyalam, S., and Thanedar, P., "Some Practical Aspects of Shape Optimization and its Influence on Intermediate Mesh Refinement," *Finite Elements in Analysis and Design*, Vol. 15, 1993, pp. 125–133.

[10]Babuska, I., and Rheinboldt, W. C., "A-Posteriori Error Estimates for the Finite Element Method," *International Journal for Numerical Method in Engineering*, Vol. 12, 1978, pp. 1597–1615.

[11]Kelly, D. W., De S. R. Gago, J. P., and Zienkiewicz, O. C., "A Posteriori Error Analysis and Adaptive Processes in the Finite Element Method: Part I—Error Analysis," *International Journal for Numerical Methods in Engineering*, Vol. 19, 1983, pp. 1593–1619.

[12]Szabo, B. A., "Some Recent Developments in Finite Element Analysis," *Computers and Mathematics with Applications*, Vol. 5, 1978, pp. 99–115.

[13]Zhang, S., and Belegundu, A. D., "Mesh Distortion Control in Shape Optimization," *AIAA Journal*, Vol. 31, No. 7, 1993, pp. 1360–1362.

[14]Bugeda, G., and Oliver, J., "A General Methodology for Structural Shape Optimization Problems Using Automatic Adaptive Remeshing," *International Journal for Numerical Methods in Engineering*, Vol. 36, 1993, pp. 3161–3185.

[15]Francavilla, A., Ramakrishnan, C. V., and Zienkiewicz, O. C., "Optimization of Shape to Minimize Stress Concentration," *Journal of Strain Analysis*, Vol. 10, No. 2, 1975, pp. 63–70.